

# Custom-sized graphene oxide for the hydrolysis of cellulose

E. Frecha, D. Torres, I. Suelves, J.L. Pinilla\*

Instituto de Carboquímica, CSIC. C/ Miguel Luesma Castán, 4, 50018, Zaragoza, Spain



## ARTICLE INFO

### Article history:

Received 20 November 2020

Received in revised form

11 January 2021

Accepted 12 January 2021

Available online 18 January 2021

### Keywords:

Graphene quantum dots

Graphene oxide

Carbocatalysts

Cellulose hydrolysis

Mix-milling

## ABSTRACT

Carbon nanostructures have attracted a long-lasting interest in cellulose hydrolysis reaction. Herein, the usefulness of catalyst downsizing is addressed using various graphene oxide (GO) morphologies, including nanofibers (GONF), sheets of few-layers (FLGO) and quantum dots (GOQD). Such materials were obtained from carbon nanofibers by oxidative cutting and subsequent exfoliation and fractioning in size. The synthesis process incorporated numerous active species (S- and O- functional groups) onto the carbon  $sp^2$ -network, whose relative abundance was in some instances tuned by hydrothermal reduction. Chemical and structural analysis of GO materials was performed by XRD, TEM, XPS and elemental analysis. GOQDs, as the smallest particle size GO material, exhibited the highest catalytic activity. However, its behaviour was dependent on the crystalline features of the starting cellulose and the substrate-catalysts interaction degree. Thus, only 17.8% of raw cellulose was depolymerized into sugars after 24 h at 135 °C, which rose to 60.1% upon enhancing its reactivity by ball-milling (8h, 600 rpm). A simple mix-milling of the cellulose with the catalyst for 10 min enabled an effective solid-solid contact, affording complete conversion and 83.5% of glucose. In comparison, 71.3% and 60.4% of glucose was obtained from their sister counterparts: FLGO and GONF, respectively.

© 2022 The Authors. Published by Elsevier Ltd. This is an open access article under the CC BY license (<http://creativecommons.org/licenses/by/4.0/>).

## 1. Introduction

In the framework of second-generation bio-refinery, the robust nature of cellulose represents a bottleneck for its effective utilization [1–3]. A hierarchical architecture, devised for providing plants structural protection, determines such chemical inertness. At a molecular level, cellulose is composed of anhydrous glucose units connected through  $\beta$ -(1 → 4)-glycosidic linkages. Linear glucan chains are organized in parallel sheets; hold together by an array of physical and chemical interactions: van der Waals,  $\pi$ - $\pi$  and hydrophobic forces as well as an extensive H-bonding network formed between adjacent OH groups. This tight internal packaging creates a rigid supramolecular structure, resistant to hydrolysis and insoluble in most solvents (water including) [4,5] even though its amorphous regions are more reactive than those highly crystalline [6,7]. The crystalline-to-amorphous transition occurs in hot and compressed water at around 320 °C and 25 MPa, driven by a series of changes induced at high temperature on both solvent and solid properties. Once in an amorphous state, cellulose is fully dissolved and hydrolyzed within a flash term (93.3% of conversion in 9.9 s), although a large fraction of the sugars ends up forming degradation

compounds (84.6%) [8]. Conversely, the hydrolysis kinetic can surmount the sugars decomposition rate and increase the yield of hydrolysis products up to 77% by raising the temperature at supercritical conditions (400 °C, 25 MPa) at low residence time (0.05 s) [9]. Whatever pathway prevails, only specific reactor configurations afford runs at such short-time scale.

Cellulose crystallinity can also be effectively deconstructed by dissolution in ionic liquids, molten salts or mineral acids [7,10–12] but its use always faces environmental and operational issues related to equipment corrosiveness, product recovery and catalyst recycling [13–15]. In search for more sustainable approaches, many catalytic systems based on solid acids were proposed for the processing of biomass [16–18]. However, the structural features of cellulose place an important physical barrier against the solid catalyst contact, whereby the steric hindrance and mass transport effects usually control the transformation [2,17,19]. For this reason, heterogeneous process schemes often include an additional pre-treatment stage of cellulose, aimed to weaken its hydrogen bond network and enhance its reactivity. The activation by swelling, mechanical comminution, ball-milling or the immersion in diluted acids are among the techniques most commonly referred [20–22]. Noteworthy, catalytic results are not only influenced by the pre-treatment method applied but also by the work-up procedure. Thus, a notorious improvement in the hydrolysis was reported by Kobayashi et al. when the cellulose and a weakly-acid carbon

\* Corresponding author.

E-mail address: [jlpinilla@icb.csic.es](mailto:jlpinilla@icb.csic.es) (J.L. Pinilla).



catalyst (K26) were ball-milled together. This practice, termed as “mix-milling”, was significantly more effective than the single-milling of cellulose or using trace hydrochloric acid in the reaction media (0.012 wt%) [23]. Quantitatively, the yield of glucans (*viz.*, the sum of glucose and oligosaccharides) after 20 min at 180 °C was 7 and 2.4-fold higher than that of the individually-milled one treated in neat and slightly acidic water, respectively [24]. Yet, resolving the contact limitations between both solid reactants by ball-milling may be time-consuming and energetically intensive.

Tailoring the catalyst surface chemistry is another alternative to promote its affinity for the substrate and enhanced the interaction with each other [8,25–28]. In this line, Suganuma *et al.* prepared an amorphous carbon bearing with  $-\text{SO}_3\text{H}$ ,  $-\text{OH}$  and  $-\text{COOH}$  groups by sulfonation of a partially carbonized organic precursor for the saccharification of crystalline cellulose [25]. The catalytic performance of this material (64% of soluble  $\beta$ -1,4 glucans; 4% of glucose) exceeded other conventional acid solids like H-mordenite, niobic acid, Nafion and Amberlyst-15. Moreover, its apparent activation energy value (110 kJ/mol) was estimated inferior to that for sulfuric acid (170 kJ/mol), which was ascribed to a stronger adsorption ability for the substrate and the co-existence of both hydrophilic sites and hydration-tolerant sulfonic groups [25]. A cellulase mimetic catalytic system, comprising binding domains and hydrolyzing centers, was proposed to understand the cooperative effect of the different surface functionalities. In this scheme, oxygen-containing groups (alcohols, epoxides or carboxylates) help to disrupt the hydrogen bond network between cellulosic chains, increasing the accessibility of the  $\beta$ -(1  $\rightarrow$  4)-glycosidic bonds for its scission by Brønsted acidic groups ( $-\text{SO}_3\text{H}$ ) [2]. This catalytic concept has inspired many other authors in their catalyst formulations [29–32], suggesting that design parameters such as the acid site density and their acid strength, surface area and the accessibility of active sites may also influence on the catalyst performance [3,17,33,34]. The role of the textural features was disclosed by Zhao *et al.* over a lamellar structure of graphene oxide (GO) decorated with abundant oxygen-functionalities, which were directly grafted during the synthesis process [33]. Thus, the full exposure to the catalytic centers only was attained once the carbon sheets were exfoliated and layered into a two-dimensional arrangement (49.9% of glucose and 58.6% of cellulose conversion after 24 h and 150 °C *vs.* 39.4% of glucose and 51.1% of cellulose conversion from the oxide graphite parent) [33]. The flexibility of graphene sheets can also facilitate the close proximity of different groups to work synergistically [35]. Using a similar GO-based catalytic system and microwave radiation (MW) as the heating source, Mission *et al.* were able to shorten the reaction time within 60 min (200 W and 180 °C) while maintaining the glucose level at 61% [36]. This value could be increased up to 73% upon a proper parametric optimization in terms of MW power density.

A series of genuine catalytic advantages seems to be unfolded as gradual downscaling on carbon nanostructures from three-to one-dimensional architectures, although their systematic study is still missing. One step downward this rank, graphene quantum dots (GQD) arise. This carbon allotrope can be defined as small planar pieces of graphene with nanometer lateral dimensions (below 100 nm) and monolayer thickness (less than ten layers) [37]. Structurally, graphene oxide quantum dots (GOQD), a material obtained after a top-down process involving oxidative cutting with acids and strong oxidants, represent an ideal catalytic template, providing large surface area, abundant active sites (edges, functional groups, etc.) and tunable surface chemistry [38]. Its excellent aqueous dispersibility, along with the opportunity of reuse, allows them to work on the borderline between the homogeneous and heterogeneous conditions. This *quasi*-homogeneous behavior was

recently highlighted by Chen *et al.* for the one-pot conversion of carbohydrates into 5-hydroxymethylfurfural (5-HMF) [39]. The aforementioned work is, to the best of our knowledge, the first catalytic application of GOQD in biomass conversion reactions, whose use promises to overwhelm other carbon materials reported thus far. More tentatively, a possible permeation inside the cellulosic matrix could be expected from its dimensionless character, aiding to suppress mass diffusion limitations and enhancing the catalytic efficiency.

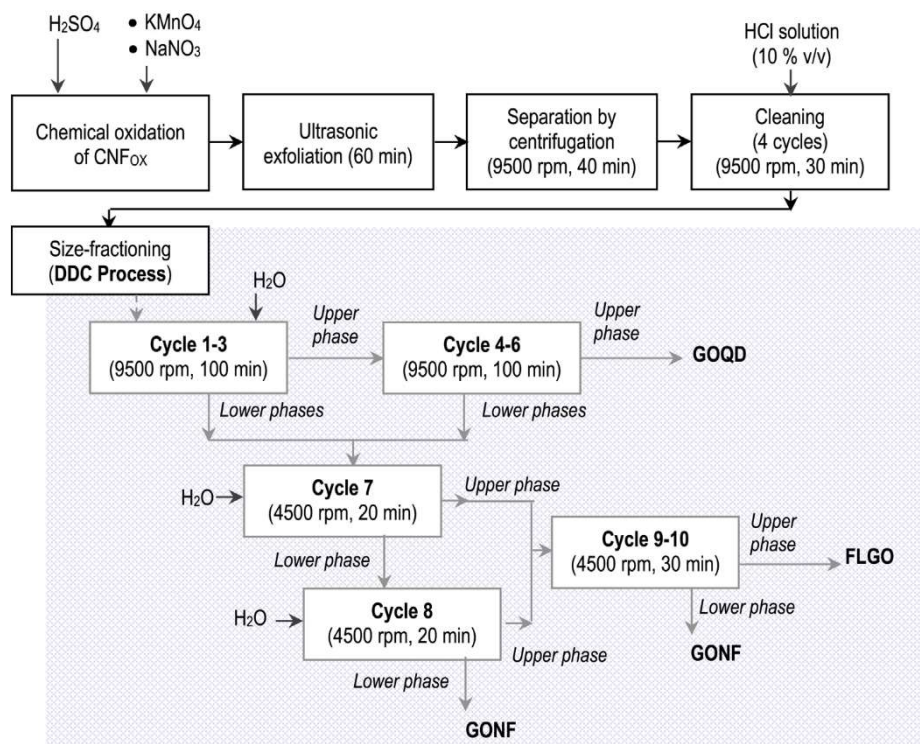
Filling in this gap, this work explores for the first time the potential of GOQD as carbocatalyst in the hydrolysis of cellulose. On the benchtop, new insights into the reactant features which steer the interaction between the glycosidic linkages of cellulose and the active sites of the solid catalyst are gained. The former is addressed from a double perspective: either by the use of cellulose with different crystallinity degree or throughout the use of catalysts with different morphology, size and functionalization degree: graphene oxide nanofibers (GONF), few-layer graphene oxide (FLGO) and graphene oxide quantum dots (GOQD).

## 2. Experimental

### 2.1. Catalyst synthesis

GONF, FLGO and GOQD were obtained from the oxidative cutting of carbon nanofibers (CNF) following a synthesis protocol previously described by our research group [40]. Briefly, CNF (fishbone-type) were grown for 180 min by catalytic decomposition of biogas ( $\text{CH}_4/\text{CO}_2$  1:1 v/v) over a  $\text{Ni}/\text{Al}_2\text{O}_3$  catalyst at 600 °C [41]. For surface activation and purification purposes, raw CNF were refluxed in  $\text{HNO}_3$  (65 wt%, Panreac, 25 mL/g CNF) at 130 °C for 30 min. These CNF, denoted as  $\text{CNF}_{\text{ox}}$ , were subjected to chemical oxidation through a modified Hummers' method and subsequent exfoliation under ultrasound-assistance. Oxidation/exfoliation products were finally washed and fractionated by size by degressive differential centrifugation (DDC). This multi-step procedure for the catalyst preparation is depicted in Scheme 1. In practice, 3.0 g of  $\text{CNF}_{\text{ox}}$  and 3.0 g of  $\text{NaNO}_3$  (Sigma Aldrich, purity  $\geq 99.0\%$ ) are suspended in 128 mL of  $\text{H}_2\text{SO}_4$  (Panreac, 96%) and placed in an ice bath. While stirring, 29.9 g of  $\text{KMnO}_4$  (Panreac, 99%,  $\text{KMnO}_4/\text{C} = 10$ ) are carefully added ( $T^{\text{a}} < 20$  °C). The oxidation proceeds for the next 2 h at  $30 \pm 5$  °C and room temperature overnight. Afterward, 240 mL of deionized water is drop-wised ( $< 70$  °C). The mixture is aged for 60 min before being diluted in another 600 mL of deionized water. At this point, the reaction is terminated with 29.9 mL of  $\text{H}_2\text{O}_2$  (Panreac, 33%). The resulting material is exfoliated for 1 h in an ultrasonic bath and then washed with dilute HCl (10% v/v, Panreac) throughout three successive centrifugation cycles (9500 rpm, 40 min, 4 °C). The final precipitate is re-dispersed in deionized water and separated into different fractions according to a DDC process. In this step, GOQD are separated from the parent suspension after 4 cycles of 100 min at 9500 rpm and 4 °C. First, the graphene material is thrice water suspended and centrifuged. Every supernatant is collected and directly submitted to a new centrifugation step (without  $\text{H}_2\text{O}$ -addition or shaking), recovering the GOQD as supernatants. Likewise, the precipitate is divided into GONF and FLGO at a rotary speed of 4500 rpm. For this purpose, the material is two-time suspended in water and centrifuged (4500 rpm, 20 min, 4 °C). Both supernatants liquids are then consecutively centrifuged (4500 rpm, 30 min, 4 °C). The bottom and upper layers belong to GONF and FLGO, respectively. The three GO-based fractions are concentrated in a rotary evaporator (56 °C) and oven-dried (60 °C). Analogous reduced counterparts, denoted as rGOQD, rFLGO and rGONF, were obtained by hydrothermal treatment of the original fractions in a stainless steel autoclave (600 mL)





**Scheme 1.** Flowchart for the catalyst synthesis.

with Teflon lining. To this effect, 1 g sample is dispersed in 400 mL of deionized water inside a PTFE cylinder by sonication for 30 min. The suspension is treated at 180 °C for 6 h and then it is evaporated to dryness under the above-mentioned methodology.

## 2.2. Characterization techniques

A set of instrumental techniques was used in the physico-chemical characterization of each fraction: X-ray diffraction (XRD) and transmission and scanning electron microscopy (TEM, SEM) for structural and topographic information, X-ray photoelectron spectroscopy (XPS) and elemental analysis (EA) for bulk and surface chemical composition, respectively.

XRD patterns were acquired on a Bruker diffractometer (Model D8 Advance, Series 2) in step scan mode ( $2\theta = 5^\circ\text{--}80^\circ$ , step size =  $0.05^\circ$ , 4s/step) using a copper anode ( $\lambda = 1.54056 \text{ \AA}$ , 40 kV, 20 mA) and a secondary graphite monochromator as the radiation source. The accompanying DIFRAC PLUS EVA 8.0 (Bruker) software and the ICDD database were used to XRD data processing and the phases' assignment, respectively. Structural parameters such as mean crystal size ( $L_c$ ) and interlayer distance ( $d$ -spacing) were estimated from the (002) peak fit according to the Scherrer formula and Bragg's Law, in that order. The number of graphene layers ( $n$ ) is then calculated as  $[(L_c/d_{002})+1]$ .

TEM images were collected with a Tecnai F30 (FEI company) microscope with an accelerating voltage of 300 kV. The instrument is equipped with a Field Emission Gun (FEG) and SuperTwin® lens, which allow a maximum point resolution of 1.5 Å. SEM micrographs were recorded on a Hitachi S-3400 N Instrument with variable pressure up to 270 Pa.

XPS measurements were conducted on an ESCAPlus OMICRON System, equipped with a hemispherical electron energy analyzer and a dual (Al/Mg) anode. The spectrometer is operated at 15 mA and 15 kV under vacuum ( $<5 \cdot 10^{-9}$  Torr), using a non-monochromatized Mg K $\alpha$  ( $\lambda = 1253.6 \text{ eV}$ ) as the excitation

source. Survey scans were acquired between 1000 eV and 0 eV, applying a pass energy of 50 eV (20 eV for higher resolution scans). The CasaXPS software was used for spectra processing. Binding energy values are calibrated with respect to C1s position (284.6 eV referenced to  $\text{sp}^2$ -carbon network), providing accuracy within  $\pm 0.2 \text{ eV}$ .

The quantitative determination of C, O, H and S was realized by EA (FlashEA® 1112 Analyzer, Thermo Scientific) equipped with a TCD detector. Metal remnants were determined by ICP-OES by means of a SPECTROBLUE (Ametek) spectrometer. The sample is digested according to the fusion method with sodium peroxide ( $\text{Na}_2\text{O}_2$ ).

## 2.3. Cellulose pre-treatment

Prior to the reaction, commercial cellulose (Fluka, Avicel® PH-101, particle size, 50  $\mu\text{m}$ ; microcrystalline, CrI = 80%) was pre-treated by ball-milling (PM 100 CM, Retsch, Germany) using a zirconia jar (50 mL) and balls ( $\varnothing = 10 \text{ mm}$ ,  $n = 10$ ,  $\text{ZrO}_2$ ). Operation time was varied from 10 min to 8 h, according to the target crystalline features, including cool-down intervals (10 min) after every 50 min of rotation at 10 Hz (600 rpm). Mix-milled samples were similarly performed. The crystalline index (CrI) of cellulose was estimated from its XRD pattern by the peak height method [42], while the morphology of the samples was observed by SEM (Figure S1 and S2-in the Supplementary Information, SI).

## 2.4. Catalytic hydrolysis tests

Catalytic activity tests were carried out in batch mode inside a high-pressure reactor (Berghof Products, BR-40 series, 45 mL) equipped with a temperature controller (BTC-3000) and a magnetic drive stirrer. In a typical run, cellulose (50 mg), catalyst (50 mg) and water (20 mL) are placed inside the reaction vessel and ultrasonically dispersed for 90 min. The system is then sealed and repeatedly

**Table 1**  
Bulk and surface catalyst composition.

	EA (wt.%)				XPS (at.%)		
	C	O	S	H	C	O	S
CNF <sub>ox</sub> <sup>a</sup>	95.6	3.12	0.02	0.34	94.05	5.95	—
GONF	50.1	45.63	1.92	2.35	70.49	27.01	2.46
FLGO	48.4	47.17	2.10	2.33	76.03	22.43	1.37
GOQD	36.4	54.67	6.09	2.84	66.51	27.83	5.56
rGONF	67.4	28.20	3.08	1.32	78.08	18.59	3.27
rFLGO	64.3	31.45	2.90	1.39	73.81	20.91	5.19
rGOQD	43.5	45.46	8.59	2.45	67.13	24.59	8.27

<sup>a</sup> Containing 0.76% of metal residue (i.e. 0.17% of Ni and 0.31% of Al in the Al<sub>2</sub>O<sub>3</sub> form) by ICP-OES.

fluxed with N<sub>2</sub> gas. The hydrolysis reaction takes place under stirring (1400 rpm) and autogenous pressure at the set temperature (135–150 ± 3 °C) and time-length (18–30 h). Zero-point is

considered when the set-point temperature is reached. At the end of the test, the reaction is rapidly stopped by quenching the system in a cool water bath. Unconverted cellulose and the catalyst are recovered by vacuum filtration (glass microfibre, 1.0 µm, Whatman®), dried (60 °C) and weighted. The pH of the final solution is measured by employing a pH electrode GLP 21<sup>+</sup> (Crison). A global diagram displaying the most relevant stages of the process can be found in the SI (Scheme S1).

## 2.5. Product analysis

Water-soluble products were analyzed by liquid chromatography (HPLC) fitted with a refractive index detector (Jasco RID-2031) and a strong cation-exchange resin column (Reprogel Pb, 9 µm, 8 × 300 mm, ReproGel®, Maisch) preceded by a guard-column. The separation is achieved within 56 min by isocratic elution of 50 µL sample at 80 °C using ultrapure H<sub>2</sub>O as mobile phase (0.055 µS/cm, 0.5 mL/min). The cell temperature was set to 30 °C. Routinely, the solution is re-filtered before the injection through a 0.45 µm PTFE

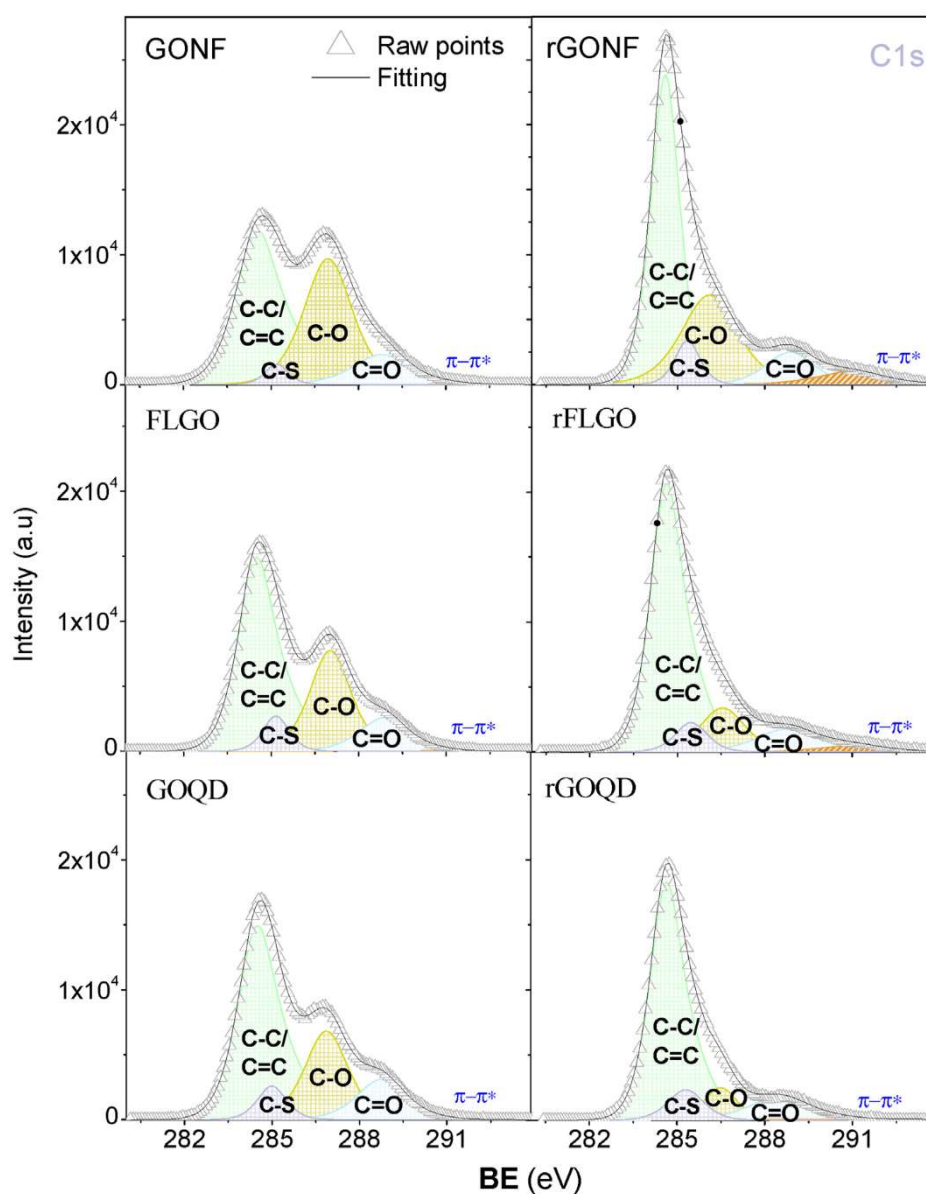


**Fig. 1.** C1s XPS spectra before (left) and after (right) hydrothermal reduction. (A colour version of this figure can be viewed online.)



**Table 2**

Chemical state of oxygen and sulphur species determined by XPS.

	C1s speciation					S2p speciation	
	C–C/C=C (284.6 eV)	C–O; (286.9 eV)	O–C=O (289.0eV)	$\pi-\pi^*$ (291 eV)	C–S (285.2eV)	–SO <sub>3</sub> H (268.4 eV)	C–SO <sub>2</sub> –C(267.6 eV)
CNF <sub>ox</sub>	62.90	30.90	2.72	3.48	—	—	—
GONF	44.45	40.68	11.49	0.24	3.14	94.62	5.38
FLGO	51.29	29.80	11.93	0.18	6.60	96.80	3.19
GOQD	52.73	26.57	13.84	0.10	6.77	95.12	4.88
rGONF	51.72	27.52	9.79	5.44	5.53	95.90	4.10
rFLGO	64.52	14.71	10.48	3.29	7.01	94.47	5.53
rGOQD	67.26	9.14	12.28	1.96	9.36	97.22	2.79

syringe filter. Calibration was done by the external standard method, using calibration curves of commercial analytical standards.

Product yield (Y) is calculated on its mass ratio basis with respect to the initial cellulose:

$$Y (\%) = (\text{mass of product})/(\text{mass of fed cellulose}) \times 100$$

The formation of large polymeric compounds, including partially hydrolyzed oligosaccharides and humins from sugars degradation routes is estimated through an indirect method. For this purpose, a given volume of filtrate solution (9 mL) is oven-dried at 75 °C to constant mass. The difference between this value (accounting for the total of non-volatile substances) and the

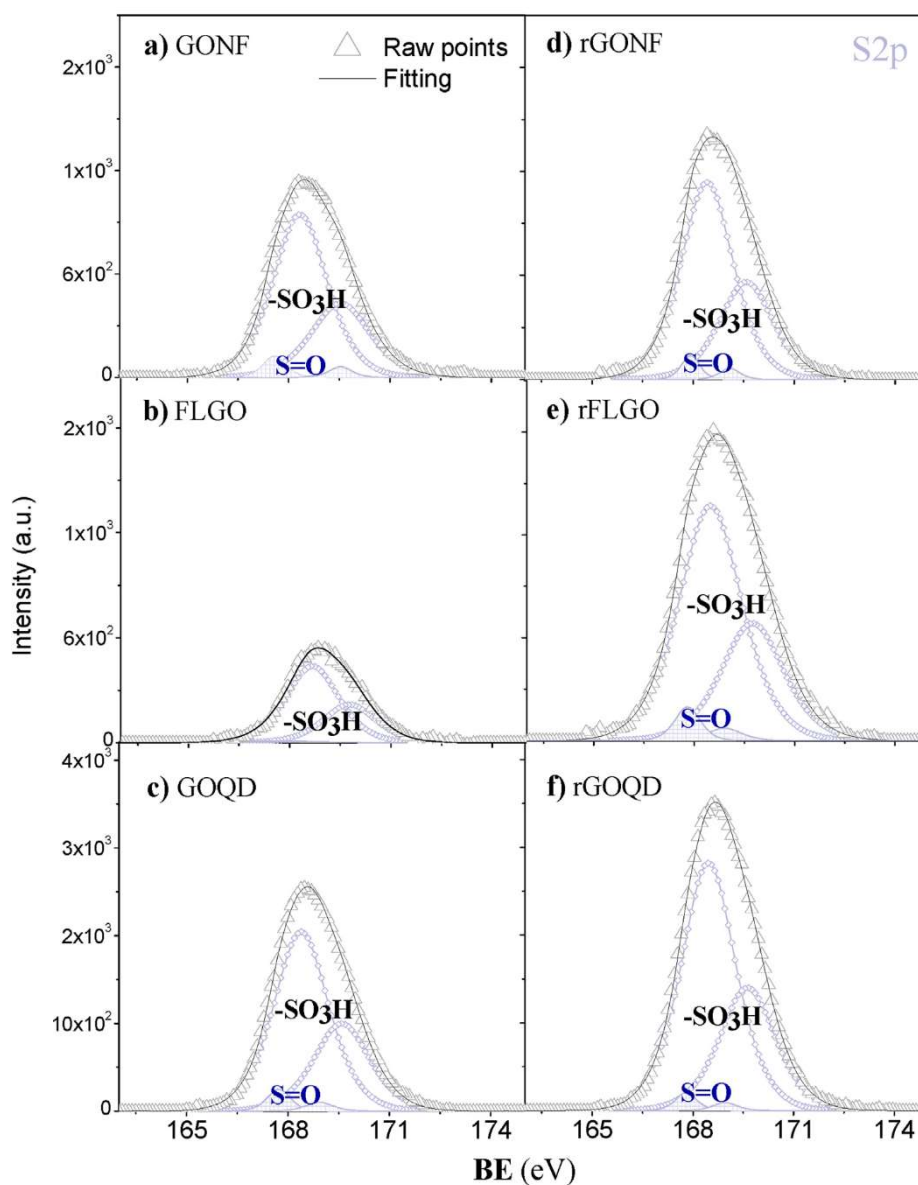


**Fig. 2.** S2p XPS spectra for the set of catalysts before (left) and after (right) hydrothermal reduction. (A colour version of this figure can be viewed online.)

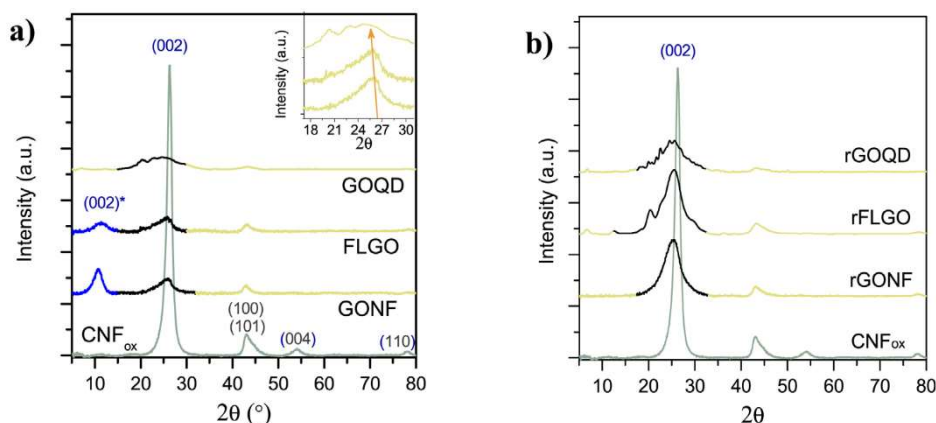


**Fig. 3.** XRD diffraction patterns of the starting graphitic precursor (CNF<sub>ox</sub>) and derived GO-based materials in the original form (a) and after hydrothermal reduction (b). (A colour version of this figure can be viewed online.)

sum of chromatographic products above the water boiling point was ascribed to this type of macromolecular complexes. Cellulose conversion (X) is expressed as the total yield of the soluble product. The moisture content in the substrate was individually considered and taken into account in the mass balance (4.8% as mean value).

### 3. Results and discussion

#### 3.1. Catalyst characterization

CNF<sub>ox</sub> used as graphenic precursor was primarily composed of carbon (95.6 wt%) and small amounts of oxygen (3.1 wt%), as it is revealed from combustion chemical analysis (Table 1). Minute amounts of metal residue (0.76 wt%, determined by ICP-OES) remain still embedded onto the carbon filamentous upon the acid washing stage. The subsequent chemical treatment with H<sub>2</sub>SO<sub>4</sub> and KMnO<sub>4</sub> introduced a large number of oxygenated and sulphur moieties onto the carbon backbone, showing those smaller fractions a higher oxidation degree. The oxygen content per weight of catalyst accounted up to 45.6, 47.2 and 54.7% in GONF, FLGO and GOQD and 1.92, 2.10 and 6.09% of sulphur, respectively. All the samples underwent partial reduction after the hydrothermal treatment, leaving behind the most unstable oxygen groups with no obvious loss of sulphur. As a result of such compositional changes, the reduced samples are enriched in S and C (Table 1). The identity of these species near the surface was inspected by XPS. The form and broadness of C1s core level profile reflect the presence of various coordination environments for carbon atoms (Fig. 1). This region was deconvoluted into five main components: an asymmetric peak at 284.6 eV combining aromatic (C=C, sp<sup>2</sup>) and

aliphatic carbon (C–C, sp<sup>3</sup>); C–O bonds (hydroxyls/epoxides, 286.5 eV), C=O bonds (carbonyl/carboxylic groups, 288.5 eV), C–S linkages (285.2 eV) and the  $\pi$ - $\pi^*$  shake-up feature (291.0 eV) [43,44]. Hydroxyl and epoxide groups are preferentially located on the basal plane whereas lactones species, carboxylic acids and ketones would predominate on the edges, according to the Lerf-Klinowski model [45–47]. The three fractions shared similar C1s envelope, but a different contribution from each species (listed in Table 2). In principle, a higher atomic percentage of both C–C/C=C bonds can be noted as downsizing on the carbon nanostructures, coming from hidden layers which are exposed upon the exfoliation of graphenic planes. Meanwhile, the relative proportion of in-plane oxygenated groups (C–O–C/C–OH) species could be overshadowed by a larger number of edge functionalities (C=O, O=C–OH), concomitant to a higher edge to basal planes ratio. The edge to basal planes ratio inversely increases with the size of GO, so that the proportion of oxygenated out-plane groups become more significant as the graphene domain size is smaller. Irrespective of the sample, the speciation of S2p XPS spectra (spin-orbit splitting of 1.1 eV, intensity ratio  $I_{1/2}/I_{3/2} = 1:2$ ) is described by a major component at around 168.4 and 169.5 eV, signature of –HSO<sub>3</sub> groups, and minor portions of sulphur at lower oxidation state (S=O, 167.3 eV) (Fig. 2) [48,49]. The presence of C–S chemical bonds, arisen at C1s core-level, is indicative that S species were covalently linked onto the carbon frame rather than forming –O–SO<sub>3</sub>H connections via etherification with oxygen atoms [35].

After reduction, the loss of most labile oxygen functionalities decreased the peak signals correspondent to (C–O), while the sp<sup>2</sup>-conjugated graphene network (and its inner  $\pi$ - $\pi^*$  transition) is restored. More resilient toward the hydrothermal stage seems sulphur and carboxylic species, remaining almost unaffected.

The oxidation degree of each fraction was closely related to their structural features, established by XRD (Fig. 3). Given the multilayer graphitic nature of the starting precursor, CNF<sub>ox</sub> exhibited a sharp diffraction peak at  $2\theta = 26.36^\circ$  characteristic of the graphite (002) plane reflection, and a set of broader signals at  $2\theta = 43.2^\circ$ ,  $45.2^\circ$ ,  $53.8^\circ$  and  $78.5^\circ$  indexed to their (100), (101), (004) and (110) faces, respectively. The (002) peak position and its width diffraction line define an average nanosheet size ( $L_c$ ) of 6.89 nm with a basal spacing ( $d$ ) of 0.338 nm between layers ( $n = 21.4$ ). The stacked structure remained on GONF which doubles its interlayer distance ( $d = 0.813$  nm) to accommodate the multiple O- and S-functionality within their sheets. The progressive oxidation further breaks the carbon lattice into smaller sp<sup>2</sup> domains and separates the graphene sheets. The exfoliation extent is evidenced by a lower

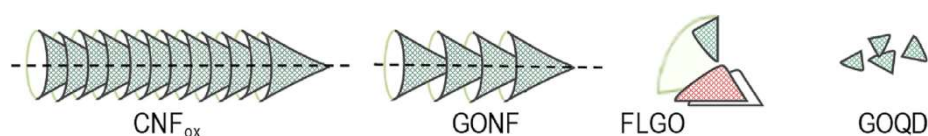
**Table 3**

Structural parameters determined by XRD from (002) and (002)\* peak position: interplanar spacing,  $d$ ; crystallite size,  $L_c$  and number of layers,  $n$ .

Catalyst	$2\theta$ (°)		$L_c$ (nm)		$d$ (nm)		$n$	
	(002)	(002)*	(002)	(002)*	(002)	(002)*	(002)	(002)*
CNF <sub>ox</sub>	26.36	–	6.89	–	0.338	–	21.4	–
GONF	25.93	10.87	1.86	3.19	0.343	0.813	6.4	4.9
FLGO	25.97	11.19	1.84	1.67	0.343	0.790	6.4	3.1
GOQD	24.38	–	0.52	n.d. <sup>a</sup>	0.365	–	2.4	<2 <sup>a</sup>
rGONF	25.24	–	1.81	–	0.352	–	6.1	–
rFLGO	25.51	–	1.54	–	0.349	–	5.4	–
rGOQD	25.22	–	1.10	–	0.353	–	4.1	–

<sup>a</sup> Below the detection limit of the instrument.





**Scheme 2.** Graphical representation of different carbon nanostructures.

number of layers in the GO materials ( $n = 4.9$  and  $3.1$  for GONF and FLGO, respectively). Table 3 compiles the evolution of all these structural parameters while the graphical representation of each nanostructure is outlined in Scheme 2. Overall, the (002) peak position shifted to (002)\*,  $2\theta = 10.8\text{--}11.2^\circ$  as the interlayer spacing was expanded whereas their diffraction lines were vanished with decreasing on the crystal size, ranging from  $3.19$  or  $1.67$  nm for GONF and FLGO, respectively, to below the detection limit for GOQD. Remains of pristine graphite are simultaneously present over all GO samples, displaying a slight enlargement of their  $d$ -spacing from GONF to GOQD (Inset of Fig. 3a). Despite this bimodal character, the structural inheritance from the parent CNF do not exceed the  $1.86$  nm in size (shown by GONF). On the contrary, the (002) plane emerges on a series of partially reduced samples, pointing towards certain graphitic re-ordering (Fig. 3b).

The morphological appearance of GO and rGO sample series was inspected by TEM (Fig. 4). GONF (a) and rGONF (d) maintained

part of the filamentous structure of the starting CNF (Figure S3). Due to the oxidation/exfoliation process, these expanded nanofilaments had a lower aspect ratio (length/width) than that of the CNF sample. FLGO (b) and rFLGO (e) were arranged into shorter graphene (or GO) domains of few layers (Fig. 4 a-b). The layer stacking can be observed for both fractions. In turn, GOQD (c) and rGOQD (f) exhibited a membrane-like structure with wrinkled features, whose transparency suggests its thin thickness. According to a previous work, this “membrane” would be composed of small overlapped  $sp^2$  carbon domains [40]. In general, micrographs of rGO samples resemble those original ones, with a certain level of aggregation and well-aligned orientation (Fig. 4 d-f). Since GO fractions were separated in size by centrifugation, their reduced counterparts maintained the same trend in size and aspect ratio.

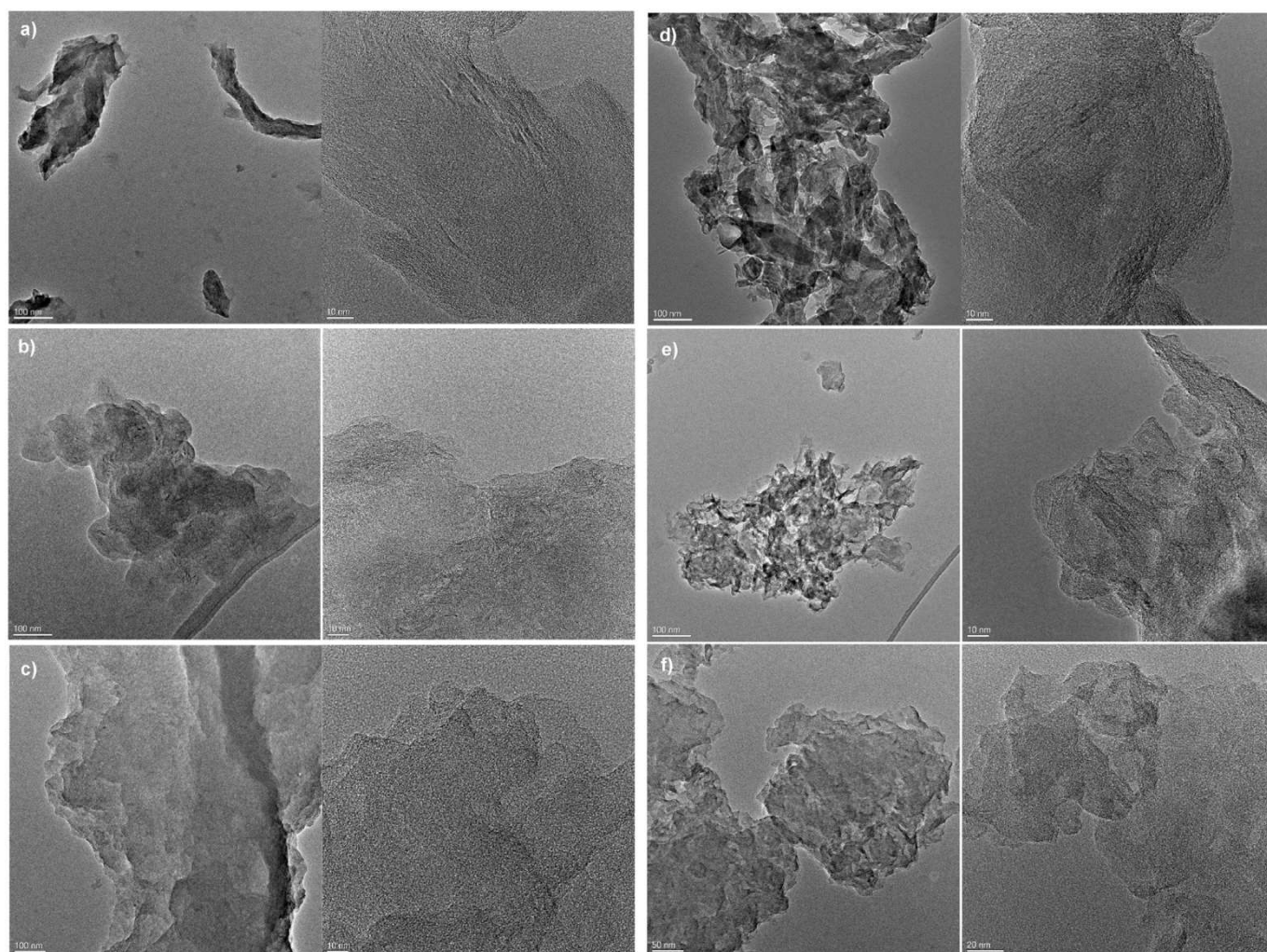
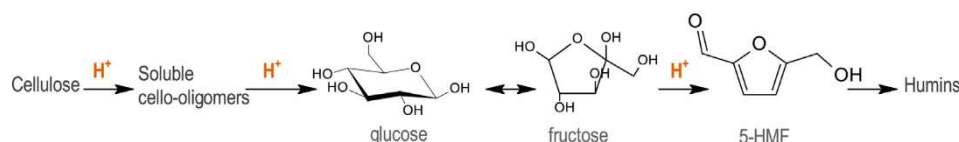


**Fig. 4.** TEM images of GO and rGO materials: a) GONF; b) FLGO; c) GOQD; d) rGONF; e) rFLGO; and f) rGOQD.





Scheme 3. Reaction network for the conversion of cellulose into glucose.

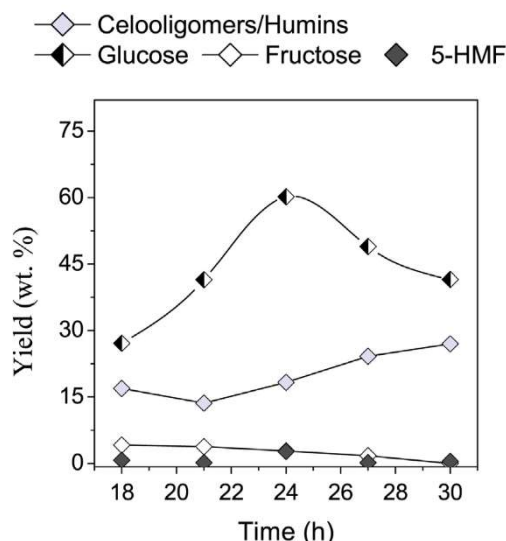


Fig. 5. Time-resolved product profiles during amorphous cellulose hydrolysis over GOQD at 135 °C.

### 3.2. Catalytic activity

A critical point in cellulose hydrolysis reaction lies in setting proper experimental conditions, aimed to control the delicate balance between the cellulose depolymerisation and the sugars degradation rates [50]. The succession of cascade reactions is illustrated in Scheme 3. In order to ascertain this issue, it was started from the most favourable situation, i.e., using ball-milled cellulose (amorphous) and GOQD as the catalyst. The hydrothermal stability of glucose in contact with a sulfonated activated carbon catalyst (AC-SO<sub>3</sub>H) for 24 h was previously investigated by Onda et al. [51]. In that work, glucose yield increased with temperature in the range of 130–160 °C, while several side reactions were promoted at higher temperature values [51]. On this basis, runs of 24 h at 150 °C have been established as typical benchmark conditions for hydrolysis tests mediated by carbon-based materials, employing catalyst doses equal to the substrate [52,53]. In our

**Table 4**  
Catalytic results for the hydrolysis of amorphous cellulose (ball milled for 8 h at 600 rpm) over different GO-based materials. (Reaction conditions: 135 °C, 24h).

Entry	Catalyst	Conversion (%)	Product distribution (wt. %)			
			Glucose	Fructose	5-HMF	Others <sup>a</sup>
1	Blank	2.1	0.2	0.0	0.0	1.9
2	CNF <sub>ox</sub>	6.9	0.2	0.0	0.0	6.7
3	GONF	70.0	50.7	3.6	1.0	14.7
4	FLGO	73.6	33.9	5.9	2.0	31.7
5	GOQD	83.9	60.1	2.8	2.7	18.3
6	rGONF	54.7	33.3	3.0	0.2	18.2
7	rFLGO	34.8	26.6	0.6	4.2	3.4
8	rGOQD	71.0	43.9	0.0	1.0	26.1

<sup>a</sup> Including cello-oligomers and humins.

reaction system, however, only 16.6% of the glucose was recovered from the reaction media under the above-mentioned conditions, whereas the extensive formation of dark-brown furan-compounds (humins) become apparent (42.9%) (data not shown). In this case, the caramelization of the sugars into insoluble by-products could be misleading the cellulose conversion measurement (66.5%) and it may be initiated by the acidity of the solution (pH~2.5), which arises from the dissociation of catalyst functionalities in the aqueous phase. Glucose susceptibility towards decomposition was limited by softening the reaction temperature down to 135 °C, albeit its profile was dependent on the residence time (Fig. 5). Specifically, the glucose concentration was linearly accumulating into the reaction medium as the reaction occurred and it reached a maximum of 61.4% after 24 h when 83.9% of cellulose was converted. Longer reaction time decreased the glucose yield in favour of dehydration products (5-HMF) and poly-condensed compounds. Therefore, 135 °C and 24 h were established as the reference conditions for subsequent runs.

In comparison with their GO relatives, GOQD exhibited the highest catalytic performance (Table 4). In particular, the cellulose conversion increased in the sequence GONF (70.0%) < FLGO (73.6%) < GOQD (83.9%), although no order was followed by the glucose yield: 50.7%, 33.9% and 60.1% (Table 4, Entry 3–5). Almost no cellulose conversion (2.1%) was noted in control experiments without catalyst (Entry 1), which appears to be partially dissolved into cello-oligomers (1.9%). This result neglects any hydrolytic contribution from hydrothermal conditions or the ball-milling stage. Moreover, nor important catalytic activity was noted for the CNF<sub>ox</sub> parent (6.94% of cellulose conversion and no glucose detected), which is consistent with its poor oxidation degree and the lack of strong acid groups (–HSO<sub>3</sub>).

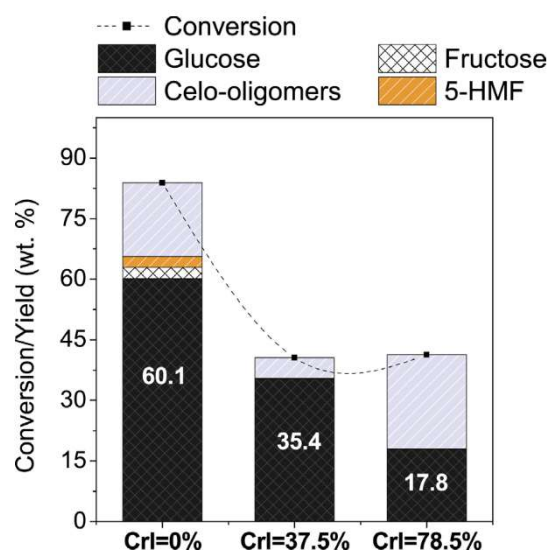
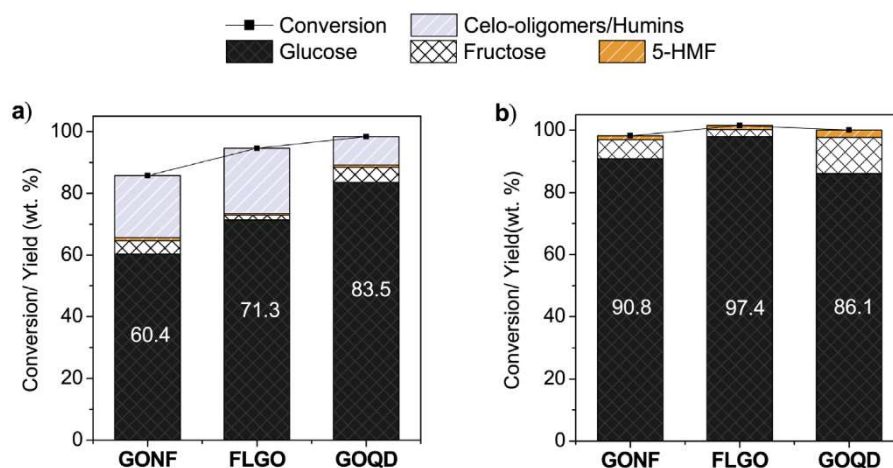


Fig. 6. Catalytic activity of GOQD as a function of the cellulose crystallinity index (CrI). Reaction conditions: 135 °C, 24h. (A colour version of this figure can be viewed online.)





**Fig. 7.** Catalytic activity of different graphene oxide mix-milled with cellulose for 10 min (a) and 120 min (b). Reaction conditions: 135 °C, 24h. (A colour version of this figure can be viewed online.)

As stated above, thermal/acid boundary conditions render glucose molecules very reactive, which preclude any attempt to reach the integral hydrolysis of cellulose by increasing the reaction time or temperature. Conceivably, a possible imbalance in the catalyst composition, that is, a higher density of strong acid sites such as  $-\text{HSO}_3$  ( $\text{pK}_a$  of ca.  $-2.8$ ) than the weakly-acidic ones like  $-\text{OH}$  and  $-\text{COOH}$  groups ( $\text{pK}_a$  of ca.  $4.7$  and  $10$ , respectively), shall favour the hydrolytic kinetic over other sugars degradation routes [54]. Such disproportion onto the functional groups can rightly be tuned by hydrothermal reduction. Nonetheless, a steep decreased in their catalytic activities was noted for all the reduced fractions (Table 4, Entry 6–8), highlighting the importance of the hydroxyl groups in the catalysts-to-substrate interaction. The instrumental role of  $-\text{OH}$  groups, serving as cellulose binders, has been earlier emphasized in the literature [55]. To illustrate this, Chen et al. reduced the hydrophilicity index of sulphonated graphene quantum dots from  $2.86$  to  $2.62$  by blocking  $-\text{OH}$  groups by silylation. The catalytic activity dramatically decreased both in terms of conversion ( $91.8\%$  vs.  $69.8\%$ ) and 5-HMF yield ( $51.7\%$  vs.  $29.1\%$ ) [39]. In our research, despite disparities on cellulose conversion values (drops of  $15.3$ ,  $38.8$ ,  $12.1\%$  for rGONF, rFLGO and rGOQD), the glucose yield followed a similar trend as their original counterparts (yield of  $33.3$ ,  $26.6$  and  $42.7\%$ , respectively). No further improvement in the glucose yield was attained over rGOQD upon prolonging the reaction time up to  $30$  h (merely  $3.0\%$ , Figure S4, in the SI).

In order to assess an eventual ability of GOQD to permeate into the interior of the cellulosic matrix, the crystallinity index of the substrate was gradually increased (Fig. 6). The exponential decline in catalytic activity with cellulose CrI reveals that even using this type of morphology, the reaction is interfacial. The fact that the catalytic results are influenced by the IC<sub>r</sub> suggests that the GOQD intercalation within the cellulose structure is not fully achieved. As such, the mix-milling practice, aimed to promote effective contact between two solid reactants, is expected to be of benefit.

When the catalyst and cellulose were ball-milled together for  $10$  min at  $600$  rpm, the glucose yield rose to  $83.5\%$  (Fig. 7a), being the cellulose completely hydrolyzed. The fractions based on FLGO and GONF yielded  $71.3\%$  and  $60.4\%$  of glucose, respectively. Just under these circumstances an obvious correlation between catalytic results and the oxidation/exfoliation degree of the GO was found. Numerical distances were shortened by extending the mix-milling time from  $10$  to  $120$  min, enabling to obtain up to  $90.8$ ,  $98.0$  and  $97.7\%$  of sugars from GONF, FLGO and GOQD, respectively (see

Fig. 7b). It is interesting to note that  $11.6\%$  of glucose undergoes isomerisation reaction into fructose over GOQD, more likely due to the electron vacancies of carbon network acting as Lewis acid centers [56]. In any case, the mechanical exfoliation of carbon materials after  $2$  h of ball-milling should not be ruled out (Figure S5), which would explain the lack of relationship between the morphological and chemical characterization of the original GO materials and the sugar yields, as opposed to what happened with the  $10$  min mix-milled conditions.

#### 4. Concluding remarks

Bridging the gap between cellulose chemistry and solid acid catalysts is essential to unlock the potential of cellulose as a renewable feedstock for energy, fuels and chemicals production. Two main tools can be used to stretch the contact between reactants: favouring the accessibility of the substrate throughout the pre-treatment stage or the morphology modulation of the catalyst. An effective molecular interaction was settled by means of a soft mix-milling stage ( $600$  rpm,  $10$  min) and using a catalyst with high amounts of functional groups ( $54.7\%$  O and  $6.1\%$  S) and sterically accessible as GOQD offers. In this manner, complete conversion of cellulose and glucose yields as high as  $83.5\%$  can be attained within  $24$  h at  $135$  °C. Lower conversion levels ( $89.5\%$  and  $98.2\%$ ) and glucose percentages ( $60.4$  and  $71.3\%$ ) were obtained from FLGO and GONF fractions, respectively. Presumably, such short-run milling stage neither energetically penalizes the process nor damages the catalyst structural integrity.

#### CRediT authorship contribution statement

**E. Frecha:** Investigation, Formal analysis, Writing - original draft, preparation. **D. Torres:** Validation, Writing - review & editing. **I. Suelves:** Conceptualization, Supervision, Resources, Project administration, Funding acquisition, Writing - review & editing. **J.L. Pinilla:** Conceptualization, Supervision, Resources, Project administration, Funding acquisition, Writing - review & editing.

#### Declaration of competing interest

The authors declare that they have no known competing financial interests or personal relationships that could have appeared to influence the work reported in this paper.



## Acknowledgments

Authors are grateful for the financial support from FEDER and the Spanish Ministry of Economy and Competitiveness (Project ENE2017-83854-R). The microscopy works have been conducted in the Advanced Microscopy Laboratories (LMA) at Institute of Nanoscience of Aragón (INA). We would like to thank the LMA-INA for offering access to their instruments and expertise. Also, the assistance of Servicio General de Apoyo a la Investigación-SAI (University of Zaragoza) is acknowledged.

## Appendix A. Supplementary data

Supplementary data to this article can be found online at <https://doi.org/10.1016/j.carbon.2021.01.108>.

## References

- [1] R. Rinaldi, F. Schueth, Acid hydrolysis of cellulose as the Entry point into biorefinery schemes, *ChemSusChem* 2 (2009) 1096–1107, <https://doi.org/10.1002/cssc.200900188>.
- [2] L. Hu, L. Lin, Z. Wu, S. Zhou, S. Liu, Chemocatalytic hydrolysis of cellulose into glucose over solid acid catalysts, *Appl. Catal., B* 174 (2015) 225–243, <https://doi.org/10.1016/j.apcatb.2015.03.003>.
- [3] J.A. Geboers, S. Van de Vyver, R. Ooms, B. Op de Beeck, P.A. Jacobs, B.F. Sels, Chemocatalytic conversion of cellulose: opportunities, advances and pitfalls, *Cat. Sci. Technol.* 1 (5) (2011) 714–726, <https://doi.org/10.1039/C1CY00093D>.
- [4] M. Jarvis, Chemistry - cellulose stacks up, *Nature* 426 (2004) 611–612, <https://doi.org/10.1038/426611a>.
- [5] Y. Nishiyama, P. Langan, H. Chanzy, Crystal structure and hydrogen-bonding system in cellulose I $\beta$  from synchrotron X-ray and neutron fiber diffraction, *J. Am. Chem. Soc.* 124 (31) (2002) 9074–9082, <https://doi.org/10.1021/ja0257319>.
- [6] T. Ennaert, B. Op de Beeck, J. Vanneste, A.T. Smit, W.J.J. Huijgen, A. Vanhulsel, P.A. et al., The importance of pretreatment and feedstock purity in the reductive splitting of (ligno)cellulose by metal supported USY zeolite, *Green Chem.* 18 (7) (2016) 2095–2105, <https://doi.org/10.1039/C5GC02346G>.
- [7] S. Coseri, Cellulose: to depolymerize... or not to? *Biotechnol. Adv.* 35 (2) (2017) 251–266, <https://doi.org/10.1016/j.biotechadv.2017.01.002>.
- [8] S. Deguchi, K. Tsujii, K. Horikoshi, Crystalline-to-amorphous transformation of cellulose in hot and compressed water and its implications for hydrothermal conversion, *Green Chem.* 10 (2008) 191–196, <https://doi.org/10.1039/B713655B>.
- [9] M. Sasaki, Z. Fang, Y. Fukushima, T. Adschiri, K. Arai, Dissolution and hydrolysis of cellulose in subcritical and supercritical water, *Ind. Eng. Chem. Res.* 39 (8) (2000) 2883–2890, <https://doi.org/10.1021/ie990690j>.
- [10] S. Van de Vyver, J. Geboers, J. Pierre, B. Sels, Recent advances in the catalytic conversion of cellulose, *ChemCatChem* 3 (2010) 82–94, <https://doi.org/10.1002/cctc.201000302>.
- [11] S. Zhu, Y. Wu, Q. Chen, Z. Yu, C. Wang, S. Jin, et al., Dissolution of cellulose with ionic liquids and its application: a mini-review, *Green Chem.* 8 (4) (2006) 325–327, <https://doi.org/10.1039/B601395C>.
- [12] J. Zhang, B. Zhang, J. Zhang, L. Lin, S. Liu, P. Ouyang, Effect of phosphoric acid pretreatment on enzymatic hydrolysis of microcrystalline cellulose, *Biotechnol. Adv.* 28 (5) (2010) 613–619, <https://doi.org/10.1016/j.biotechadv.2010.05.010>.
- [13] P. Mäki-Arvela, B. Holmbom, T. Salmi, D.Y. Murzin, Recent progress in synthesis of fine and specialty chemicals from wood and other biomass by heterogeneous catalytic processes, *Catal. Rev.* 49 (3) (2007) 197–340, <https://doi.org/10.1080/01614940701313127>.
- [14] P.L. Dhepe, A. Fukuoka, Cellulose conversion under heterogeneous catalysis, *ChemSusChem* 1 (12) (2008) 969–975, <https://doi.org/10.1002/cssc.200800129>.
- [15] P.T. Anastas, J.C. Warner, *Green Chemistry: Theory and Practice*, Oxford University Press, Oxford [England]; New York, 1998.
- [16] F. Guo, Z. Fang, C.C. Xu, R.L. Smith, Solid acid mediated hydrolysis of biomass for producing biofuels, *Prog. Energy Combust. Sci.* 38 (5) (2012) 672–690, <https://doi.org/10.1016/j.pecs.2012.04.001>.
- [17] Y.-B. Huang, Y. Fu, Hydrolysis of cellulose to glucose by solid acid catalysts, *Green Chem.* 15 (2013) 1095–1111, <https://doi.org/10.1039/C3GC40136G>.
- [18] S. De, S. Dutta, B. Saha, Critical design of heterogeneous catalysts for biomass valorization: current thrust and emerging prospects, *Catal. Sci. Technol.* 6 (20) (2016) 7364–7385, <https://doi.org/10.1039/C6CY01370H>.
- [19] P.L. Dhepe, A. Fukuoka, Cellulose conversion under heterogeneous catalysis, *ChemSusChem* 1 (12) (2008) 969–975, <https://doi.org/10.1002/cssc.200800129>.
- [20] Y. Liao, B.O. de Beeck, K. Thielemans, T. Ennaert, J. Snelders, M. Dusselier, et al., The role of pretreatment in the catalytic valorization of cellulose, *Mol. Catal.* 487 (2020) 110883, <https://doi.org/10.1016/j.mcat.2020.110883>.
- [21] P. Kumar, D.M. Barrett, M.J. Delwiche, P. Stroeve, Methods for pretreatment of lignocellulosic biomass for efficient hydrolysis and biofuel production, *Ind. Eng. Chem. Res.* 48 (8) (2009) 3713–3729, <https://doi.org/10.1021/ie801542g>.
- [22] V.B. Agbor, N. Cicek, R. Sparling, A. Berlin, D.B. Levin, Biomass pretreatment: fundamentals toward application, *Biotechnol. Adv.* 29 (6) (2011) 675–685, <https://doi.org/10.1016/j.biotechadv.2011.05.003>.
- [23] H. Kobayashi, M. Yabushita, T. Komanoya, K. Hara, I. Fujita, A. Fukuoka, High-yielding one-pot synthesis of glucose from cellulose using simple activated carbons and trace hydrochloric acid, *ACS Catal.* 3 (4) (2013) 581–587, <https://doi.org/10.1021/cs300845f>.
- [24] M. Yabushita, H. Kobayashi, K. Hara, A. Fukuoka, Quantitative evaluation of ball-milling effects on the hydrolysis of cellulose catalysed by activated carbon, *Catal. Sci. Technol.* 4 (8) (2014) 2312–2317, <https://doi.org/10.1039/C4CY00175C>.
- [25] S. Suganuma, K. Nakajima, M. Kitano, D. Yamaguchi, H. Kato, S. Hayashi, et al., Hydrolysis of cellulose by amorphous carbon bearing SO<sub>3</sub>H, COOH, and OH groups, *J. Am. Chem. Soc.* 130 (2008) 12787–12793, <https://doi.org/10.1021/ja803983h>.
- [26] K. Nakajima, M. Hara, Amorphous carbon with SO<sub>3</sub>H groups as a solid Brønsted acid catalyst, *ACS Catal.* 2 (7) (2012) 1296–1304, <https://doi.org/10.1021/cs300103k>.
- [27] M. Kitano, D. Yamaguchi, S. Suganuma, K. Nakajima, H. Kato, S. Hayashi, et al., Adsorption-enhanced hydrolysis of beta-1,4-glucan on graphene-based amorphous carbon bearing SO<sub>3</sub>H, COOH, and OH groups, *Langmuir* 25 (2009) 5068–5075, <https://doi.org/10.1021/la8040506>.
- [28] A.T. To, P.-W. Chung, A. Katz, Weak-acid sites catalyze the hydrolysis of crystalline cellulose to glucose in water: importance of post-synthetic functionalization of the carbon surface, *Angew. Chem. Int. Ed.* 54 (38) (2015) 11050–11053, <https://doi.org/10.1002/anie.201504865>.
- [29] L. Shuai, X. Pan, Hydrolysis of cellulose by cellulase-mimetic solid catalyst, *Energy Environ. Sci.* 5 (2012) 6889–6894, <https://doi.org/10.1039/C2EE03373A>.
- [30] A. Shrotri, H. Kobayashi, A. Fukuoka, Air oxidation of activated carbon to synthesize a biomimetic catalyst for hydrolysis of cellulose, *ChemSusChem* 9 (11) (2016) 1299–1303, <https://doi.org/10.1002/cssc.201600279>.
- [31] D. Verma, R. Tiwari, A.K. Sinha, Depolymerization of cellulosic feedstocks using magnetically separable functionalized graphene oxide, *RSC Adv.* 3 (32) (2013) 13265–13272, <https://doi.org/10.1039/C3RA41025K>.
- [32] Q. Yang, X. Pan, Bifunctional porous polymers bearing boronic and sulfonic acids for hydrolysis of cellulose, *ACS Sustain. Chem. Eng.* 4 (9) (2016) 4824–4830, <https://doi.org/10.1021/acssuschemeng.6b01102>.
- [33] X. Zhao, J. Wang, C. Chen, Y. Huang, A. Wang, T. Zhang, Graphene oxide for cellulose hydrolysis: how it works as a highly active catalyst? *Chem. Commun.* 50 (26) (2014) 3439–3442, <https://doi.org/10.1039/C3CC49634A>.
- [34] J. Pang, A. Wang, M. Zheng, T. Zhang, Hydrolysis of cellulose into glucose over carbons sulfonated at elevated temperatures, *Chem. Commun. (J. Chem. Soc. Sect. D)* 46 (37) (2010) 6935–6937, <https://doi.org/10.1039/C0CC02014A>.
- [35] Z. Wei, Y. Yang, Y. Hou, Y. Liu, X. He, S. Deng, A new approach towards acid catalysts with high reactivity based on graphene nanosheets, *ChemCatChem* 6 (8) (2014) 2354–2363, <https://doi.org/10.1002/cctc.201402100>.
- [36] E.G. Mission, A.T. Quinlan, M. Sasaki, T. Kida, Synergizing graphene oxide with microwave irradiation for efficient cellulose depolymerization into glucose, *Green Chem.* 19 (16) (2017) 3831–3843, <https://doi.org/10.1039/C7GC01691C>.
- [37] A. Bianco, H.-M. Cheng, T. Enoki, Y. Gogotsi, R.H. Hurt, N. Koratkar, et al., All in the graphene family – a recommended nomenclature for two-dimensional carbon materials, *Carbon* 65 (2013) 1–6, <https://doi.org/10.1016/j.carbon.2013.08.038>.
- [38] Y. Yan, J. Gong, J. Chen, Z. Zeng, W. Huang, K. Pu, et al., Recent advances on graphene quantum dots: from chemistry and physics to applications, *Adv. Mater.* 31 (21) (2019) 1808283, <https://doi.org/10.1002/adma.201808283>.
- [39] K. Li, J. Chen, Y. Yan, Y. Min, H. Li, F. Xi, et al., Quasi-homogeneous carbocatalysis for one-pot selective conversion of carbohydrates to 5-hydroxymethylfurfural using sulfonated graphene quantum dots, *Carbon* 136 (2018) 224–233, <https://doi.org/10.1016/j.carbon.2018.04.087>.
- [40] D. Torres, J.L. Pinilla, E.M. Gálvez, I. Suelves, Graphene quantum dots from fishbone carbon nanofibers, *RSC Adv.* 6 (54) (2016) 48504–48514, <https://doi.org/10.1039/C6RA09679D>.
- [41] J.L. Pinilla, S. de Llobet, R. Moliner, I. Suelves, Ni-Co bimetallic catalysts for the simultaneous production of carbon nanofibres and syngas through biogas decomposition, *Appl. Catal., B* 200 (2017) 255–264, <https://doi.org/10.1016/j.apcatb.2016.07.015>.
- [42] S. Park, J.O. Baker, M.E. Himmel, P.A. Parilla, D.K. Johnson, Cellulose crystallinity index: measurement techniques and their impact on interpreting cellulase performance, *Biotechnol. Biofuels* 3 (1) (2010) 10, <https://doi.org/10.1186/1754-6834-3-10>.
- [43] H. Jeong, H.-J. Noh, J.Y. Kim, M. Jin, C. Park, Y.H. Lee, X-ray absorption spectroscopy of graphite oxide, *Europhys. Lett.* 82 (2008) 67004, <https://doi.org/10.1209/0295-5075/82/67004>.
- [44] L. Huang, H. Ye, S. Wang, Y. Li, Y. Zhang, W. Ma, et al., Enhanced hydrolysis of cellulose by highly dispersed sulfonated graphene oxide, *Bioresour. Res.* 13 (4) (2018) 8853–8870, <https://doi.org/10.15376/biores.13.4.8853-8870>.
- [45] D.R. Dreyer, A.D. Todd, C.W. Bielawski, Harnessing the chemistry of graphene oxide, *Chem. Soc. Rev.* 43 (15) (2014) 5288–5301, <https://doi.org/10.1039/C4CS00060A>.



- [46] S. Zhu, J. Wang, W. Fan, Graphene-based catalysis for biomass conversion, *Catal. Sci. Technol.* 5 (8) (2015) 3845–3858, <https://doi.org/10.1039/C5CY00339C>.
- [47] A. Lerf, H. He, M. Forster, J. Klinowski, Structure of graphite oxide revisited, *J. Phys. Chem. B* 102 (23) (1998) 4477–4482, <https://doi.org/10.1021/jp9731821>.
- [48] High resolution XPS of organic polymers: the scienta ESCA300 database (beamson, G.; briggs, D.), *J. Chem. Educ.* 70 (1) (1993) A25, <https://doi.org/10.1021/ed070pA25.5>.
- [49] M.M. Nasef, H. Saidi, Surface studies of radiation grafted sulfonic acid membranes: XPS and SEM analysis, *Appl. Surf. Sci.* 252 (8) (2006) 3073–3084, <https://doi.org/10.1016/j.apsusc.2005.05.013>.
- [50] A. Cabiac, E. Guillon, F. Chambon, C. Pinel, F. Rataboul, N. Essayem, Cellulose reactivity and glycosidic bond cleavage in aqueous phase by catalytic and non catalytic transformations, *Appl. Catal., A* 402 (1) (2011) 1–10, <https://doi.org/10.1016/j.apcata.2011.05.029>.
- [51] A. Onda, T. Ochi, K. Yanagisawa, Hydrolysis of cellulose selectively into glucose over sulfonated activated-carbon catalyst under hydrothermal conditions, *Top. Catal.* 52 (6) (2009) 801–807, <https://doi.org/10.1007/s11244-009-9237>.
- [52] A. Onda, T. Ochi, K. Yanagisawa, Selective hydrolysis of cellulose into glucose over solid acid catalysts, *Green Chem.* 10 (10) (2008) 1033–1037, <https://doi.org/10.1039/B808471H>.
- [53] S. Van de Vyver, L. Peng, J. Geboers, H. Schepers, F. Clippel, C. Gommès, et al., Sulfonated silica/carbon nanocomposites as novel catalysts for hydrolysis of cellulose to glucose, *Green Chem.* 12 (2010) 1560–1563, <https://doi.org/10.1039/C0GC00235F>.
- [54] K.-i. Shimizu, A. Satsuma, Toward a rational control of solid acid catalysis for green synthesis and biomass conversion, *Energy Environ. Sci.* 4 (9) (2011) 3140–3153, <https://doi.org/10.1039/C1EE01458G>.
- [55] Y. Wu, Z. Fu, D. Yin, Q. Xu, F. Liu, C. Lu, et al., Microwave-assisted hydrolysis of crystalline cellulose catalyzed by biomass char sulfonic acids, *Green Chem.* 12 (4) (2010) 696–700, <https://doi.org/10.1039/B917807D>.
- [56] H. Wang, T. Deng, Y. Wang, X. Cui, Y. Qi, X. Mu, et al., Graphene oxide as a facile acid catalyst for the one-pot conversion of carbohydrates into 5-ethoxymethylfurfural, *Green Chem.* 15 (9) (2013) 2379–2383, <https://doi.org/10.1039/C3GC41109E>.